Efficacy of Sunitinib and Radiotherapy in Genetically Engineered Mouse Model of Soft-Tissue Sarcoma

Citation: Yoon, Sam S., Lars Stangenberg, Yoon-Jin Lee, Courtney Rothrock, Jonathan M. Dreyfuss, Kwan-Hyuck Baek, Peter R. Waterman, et al. "Efficacy of Sunitinib and Radiotherapy in Genetically Engineered Mouse Model of Soft-Tissue Sarcoma." International Journal of Radiation Oncology*Biology*Physics 74, no. 4 (July 2009): 1207–1216.

As Published: http://dx.doi.org/10.1016/j.ijrobp.2009.02.052

Publisher: Elsevier

Persistent URL: http://hdl.handle.net/1721.1/101278

Version: Author's final manuscript: final author's manuscript post peer review, without publisher's formatting or copy editing

Published in final edited form as:
Int J Radiat Oncol Biol Phys. 2009 July 15; 74(4): 1207–1216. doi:10.1016/j.ijrobp.2009.02.052.

Efficacy of Sunitinib and Radiotherapy in Genetically Engineered Mouse Model of Soft-tissue Sarcoma

Sam S. Yoon, M.D.[*], **Lars Stangenberg, M.D.**[†], **Yoon-Jin Lee, Ph.D.**[*], **Courtney Rothrock, B.S.**[*], **Jonathan M. Dreyfuss, M.S.**[‡], **Kwan-Hyuck Baek, Ph.D.**[§], **Peter R. Waterman, B.S.**[†,¶], **G. Petur Nielsen, M.D.**[‖], **Ralph Weissleder, M.D., Ph.D.**[†,¶], **Umar Mahmood, M.D., Ph.D.**[†,¶], **Peter J. Park, Ph.D.**[‡], **Tyler Jacks, Ph.D.**[#], **Rebecca D. Dodd, Ph.D.**[**], **Carolyn J. Fisher, Ph.D.**[**], **Sandra Ryeom, Ph.D.**[§], and **David G. Kirsch, M.D., Ph.D.**[**]

[*]Department of Surgery, Division of Surgical Oncology, Massachusetts General Hospital and Harvard Medical School, Boston, MA

[‖] Department of Pathology, Massachusetts General Hospital and Harvard Medical School, Boston, MA

[†]Center for Molecular Imaging Research, Department of Radiology, Massachusetts General Hospital and Harvard Medical School, Boston, MA

[¶]Center for Systems Biology, Massachusetts General Hospital and Harvard Medical School, Boston, MA

[‡] Harvard-Partners Center for Genetics and Genomics, Brigham and Women's Hospital and Harvard Medical School, Boston, MA

[§] Vascular Biology Program and Department of Surgery, Boston Children's Hospital and Harvard Medical School, Boston, MA

[#]Center for Cancer Research, Department of Biology, and Howard Hughes Medical Institute, Massachusetts Institute of Technology, Boston, MA

[**]Departments of Radiation Oncology and Pharmacology and Cancer Biology, Duke University School of Medicine, Durham, NC

Abstract

Purpose—Sunitinib (SU) is a multitargeted receptor tyrosine kinase inhibitor of the vascular endothelial growth factor and platelet-derived growth factor receptors. The present study examined SU and radiotherapy (RT) in a genetically engineered mouse model of soft tissue sarcoma (STS).

Methods and Materials—Primary extremity STSs were generated in genetically engineered mice. The mice were randomized to treatment with SU, RT (10 Gy × 2), or both (SU+RT). Changes in the tumor vasculature before and after treatment were assessed *in vivo* using fluorescence-mediated tomography. The control and treated tumors were harvested and extensively analyzed.

Results—The mean fluorescence in the tumors was not decreased by RT but decreased 38–44% in tumors treated with SU or SU+RT. The control tumors grew to a mean of 1378 mm^3 after 12 days. SU alone or RT alone delayed tumor growth by 56% and 41%, respectively, but maximal growth

Reprint requests to: Sam S. Yoon, M.D., Division of Surgical Oncology, Massachusetts General Hospital, Yawkey 7B-7926, 55 Fruit St., Boston, MA 02114. Tel: (617) 726-4241; Fax: (617) 724-3895; E-mail: syoon@partners.org.

Conflict of interest: none.

Supplementary material and figures for this article can be found at www.redjournal.org.

inhibition (71%) was observed with the combination therapy. SU target effects were confirmed by loss of target receptor phosphorylation and alterations in SU-related gene expression. Cancer cell proliferation was decreased and apoptosis increased in the SU and RT groups, with a synergistic effect on apoptosis observed in the SU+RT group. RT had a minimal effect on the tumor microvessel density and endothelial cell-specific apoptosis, but SU alone or SU+RT decreased the microvessel density by >66% and induced significant endothelial cell apoptosis.

Conclusion—SU inhibited STS growth by effects on both cancer cells and tumor vasculature. SU also augmented the efficacy of RT, suggesting that this combination strategy could improve local control of STS.

Keywords

Sarcoma; radiotherapy; angiogenesis; sunitinib

Introduction

Soft tissue sarcomas (STSs) are a heterogeneous group of tumors derived from cells usually of mesenchymal origin. Despite aggressive surgery and radiotherapy (RT), STSs located in difficult anatomic locations or adjacent to vital structures still have a significant risk of local recurrence. Drugs can increase the efficacy of RT on tumors through effects on cancer cells, as well as effects on the tumor microenvironment. Vascular endothelial growth factor (VEGF) is overexpressed by most human cancers, and numerous preclinical studies and a few human studies have demonstrated that anti-VEGF therapies can improve the efficacy of RT (1). Sunitinib (SU11248, Sutent) is an oral, multitargeted tyrosine kinase inhibitor targeting the vascular endothelial growth factor receptors 1–3 (VEGFR1–3) and platelet-derived growth factor receptors α and β (PDGFR-α and -β) (2). We hypothesized that sunitinib (SU) would be an optimal agent to combine with RT for STSs. We had several reasons for this hypothesis. First, STSs, as with nearly all tumors, require angiogenesis to grow beyond a few millimeters, and SU targets receptors critical to endothelial cell activation and tumor angiogenesis, including VEGFRs and PDGFRs (3). Second, PDGFR-α and -β are mutated and/or overexpressed in many STSs. In our own gene expression microarray analysis comparing STSs and normal tissues, PDGFR-α expression was sevenfold greater in the STSs than in the normal tissues (4). Third, preclinical studies have demonstrated that SU enhances the effects of radiation *in vitro* (5) and in murine xenograft tumor models (6).

We recently described a genetically engineered mouse model of STSs in which intramuscular delivery of an adenovirus expressing Cre recombinase into mice with conditional mutations in K-ras and p53 resulted in primary, high-grade STS at the site of injection in >90% of mice at a median interval of approximately 80 days (7). Taking into account that human sarcomas are highly heterogeneous, sarcomas that develop in these genetically engineered mice closely resemble some human sarcomas according to the genetic and histologic analyses. Thus, we used this mouse model of STSs to examine the efficacy of SU and/or RT.

Methods and Materials

Mouse studies

The Massachusetts Institute of Technology Institutional Animal Care and Use Committee and the Subcommittee on Research Animal Care at Massachusetts General Hospital approved all animal studies and procedures. Hindlimb tumors were generated in transgenic mice with conditional mutations in oncogenic K-ras and the p53 tumor suppressor gene, as previously described (8). Once tumors reached 100–200 mm^3, they were randomized to treatment with SU, RT, both SU and RT, or carrier alone (n = 5–7 mice/group). Sunitinib suspension was

delivered by oral gavage at a dose of 40 mg/kg daily for 12 consecutive days. The mice that did not receive SU received carrier by oral gavage daily. After anesthesia, RT was delivered to the tumor-bearing hind limb using a 4-MV linear accelerator, using a total dose of 20 Gy administered in two fractions of 10 Gy on Days 4 and 5. The mice were irradiated in a plastic box so that the 4-MV beam passed through 1 cm of material (Fig. E1a). In addition, 1 cm of bolus was placed over the STS. The tumor volume was determined every 2–3 days by measuring the tumor in three dimensions and calculating the tumor volume using the following formula: tumor volume = $(A \times B \times C \times \pi)/6$. At the end of 2 weeks of treatment, the tumors were harvested.

Fluorescence-mediated tomography

Our methods and analysis of tumor vascular volume using fluorescence-mediated tomography (FMT) have been previously described (9). In brief, AngioSPARK 680 and AngioSPARK 750 probes, which are pegylated nanoparticles coupled to a near infrared fluorochrome, were purchased from VisEn Medical (Bedford, MA) for imaging of the tumor vasculature. After intravenous injection, the probes remain in the vasculature for ≤4 h. The mice were serially imaged before and after treatment. A commercially available three-dimensional FMT imaging system (VisEn Medical) was used to detect the AngioSPARK probe and to calculate the quantitative levels of fluorescence within the tumors. The FMT software was then used to calculate the mean fluorescent signal intensity.

Histologic tumor analysis

CD31 and proliferating cell nuclear antigen (PCNA) immunohistochemistry (10) and CD31 and terminal deoxynucleotidyl transferase-mediated dUTP-biotin nick end labeling (TUNEL) immunofluorescence (11) were performed, as previously described. For phospho-VEGFR-2 and phospho-PDGFR-β immunofluorescence, deparaffinized sections were treated with 10 mM citrate buffer (pH 6.0) for 20 min at 95°C and were blocked with 5% normal horse serum in 0.3% Triton-X 100/phosphate-buffered saline for 1 h. The sections were co-immunostained with mouse anti-CD31 monoclonal antibody (1:100; Pharmingen, San Jose, CA) and rabbit anti-phospho-VEGFR-2 (1:100, Cell Signaling, Danvers, MA) or rabbit anti-phospho-PDGFR-β (1:100, Cell Signaling) overnight at 4°C. After washing, the sections were incubated with goat anti-rabbit Alexa 488 (1:500, Molecular Probes, Carlsbad, CA) and goat anti-mouse Alexa 594 conjugated secondary antibody (1:500, Molecular Probes) in 0.3% Triton-X 100/phosphate-buffered saline for 1 h at room temperature. Cell nuclei were labeled with Hoechst dye (1 μg/mL). The images were obtained on a Zeiss microscope and analyzed using AxioVision, version 4.0 software (Carl Zeiss Vision, San Diego, CA).

Microarray analysis

RNA was isolated from tumor tissue using the Qiagen RNeasy kit. The samples were profiled on Illumina's MouseRef-8, version 1.1., Expression BeadChips, which contain >24,000 50-mer oligo probes. Image analysis was performed using Illumina's BeadStudio, version 3.0.14 (San Diego, CA), Gene Expression Module.

All statistical analyses were conducted using the statistical software R (available from www.r-project.org) with microarray analysis tools from the Bioconductor project (www.bioconductor.org). Five samples were excluded because, on histologic examination, a significant amount of normal muscle or other nontumor tissue was present.

Quantitative reverse transcriptase-polymerase chain reaction

For quantitative reverse transcriptase-polymerase chain reaction (RT-PCR), total RNA was isolated from tumor tissue preserved in RNA Later (Qiagen, Valencia, CA) using the RNeasy

Mini Kit (Qiagen), according to the manufacturer's instructions. RNA was isolated from cell lines *in vitro* using Trizol (Invitrogen, Carlsbad, CA) according to the manufacturer's instructions. cDNA was synthesized using the Superscript First-Strand Synthesis System (Invitrogen) with random hexamers according to the manufacturer's instructions. Quantitative real time PCR analysis was done using the LightCycler Detection System (Roche Diagnostics, Madison, WI) using 500 ng of cDNA product and LightCycler FastStart DNA Master^{PLUS} SYBR Green I, according to the manufacturer's instructions. The primers for 18S RNA were obtained from QuantumRNA Classic 18S Internal Standard (Ambion, Austin, TX). See Table E1 for primers for mouse VEGF, angiopoietin 1 and 2, basic fibroblast growth factor, PDGF-α and PDGF-β. The concentrations of 18S RNA and angiogenic factors were calculated from the crossing point using a standard curve. The relative value was then determined by the dividing the calculated angiogenic factor level by the calculated 18S level for each sample and then normalizing the data so that the lowest relative value was 1.

Statistical analysis

The treatment groups were compared using the nonparametric Kruskal-Wallis test (12).

Results

Treatment of extremity sarcomas with SU and/or RT

We recently described a mouse model of STS in which primary high-grade sarcomas could be generated under spatial and temporal control after injection of adenovirus expressing Cre recombinase (13). The primary STSs generated in these mice were used to assess the efficacy of SU and RT. A total of 24 mice with conditional mutations in p53 and K-ras were injected in the left lower extremity with adenovirus expressing Cre recombinase to generate the tumors (Fig. 1A). All mice had conditional mutations in oncogenic K-ras (LSL-Kras^{G12D}). The conditional mutations in p53 were point mutations (p53$^{LSL.R270H/FL}$ or p53$^{LSL.R172H/FL}$) or a floxed p53 allele (p53$^{FL/Fl}$). Overall, 22 mice (92%) developed extremity STSs at a median of 84 days (Fig. 1B). Once the tumors had reached approximately 100–200 mm^3, the mice were randomized to one of four treatment groups: carrier alone, SU alone, carrier and RT, or SU and RT (Fig. 1C).

Treatment effects on phosphorylation of target receptors and gene expression

To determine whether SU blocked target tyrosine kinases in the STSs *in vivo*, we harvested the tumors treated with SU or carrier alone and analyzed the tyrosine kinase receptors VEGFR-2 and PDGR-β, known targets of SU, by immunofluorescence using phospho-specific antibodies. The tumors treated with carrier alone showed positive staining for phosphorylated VEGFR-2 (Fig. 2A), suggesting activation of endothelial cell VEGFR-2 in these tumors. This staining was co-localized to both CD31 and VE-cadherin (Fig. E1b). After treatment with SU, the immunofluorescence for phosphorylated VEGFR-2 was greatly attenuated. Similarly, tumors treated with carrier alone had high levels of phosphorylated PDGFR-β, and tumors treated with SU had little or no expression of phosphorylated PDGFR-β (Fig. 2A). The tumor cells and endothelial cells usually both expressed PDGFR-β in this mouse model (data not shown).

RNA from all 22 tumors was submitted for microarray analysis using Illumina MouseRef-8 Expression BeadChips; however, five samples were excluded from analysis because of poor histologic quality (see the “Methods and Materials” section). Changes in the global gene expression patterns related to treatment were examined. Using hierarchical clustering based on the 500 most variable genes, all tumors treated with carrier alone were clustered in the same group (Fig. 2B). Three other clusters emerged from this analysis: one cluster contained tumors

treated with RT and tumors treated with both RT and SU, another cluster contained only SU-treated tumors, and a final cluster contained tumors from all three treatment groups.

Hierarchical clustering was also performed using a gene set of only 20 probes, which included receptors targeted by SU and their associated ligands (Fig. 2C). This analysis produced two clusters; one cluster contained all five tumors treated with carrier alone, along with one SU-treated tumor. The other cluster contained tumors treated with SU or RT plus SU. This analysis suggested that SU treatment was exerting effects on its target pathways. In addition to the SU-related gene set, an additional gene set related to the Gene Ontology response to RT (GO: 0009314) was analyzed. The response to the RT gene set was significantly altered in the RT vs. carrier comparison ($p = .018$) and in the RT/SU+RT vs. control comparisons ($p = 0.047$), suggesting that RT altered expression of these RT-related genes.

The microarray data were also analyzed for highly upregulated and downregulated genes. When contrasting tumors treated with SU with the control tumors, 26 genes were downregulated at least threefold and had a q value of <0.025, and 6 genes were upregulated at least threefold and had a q value of <0.025 (Table E2). The macrophage scavenger receptor 2, which has been previously demonstrated to be upregulated after colony-stimulating factor 1 treatment (14), was the most downregulated gene (12.3-fold). In addition, the colony-stimulating factor 1 receptor was downregulated 4.5-fold. Downregulations of macrophage scavenger receptor 2 was confirmed at the RNA and protein levels by quantitative reverse transcriptase PCR and Western blot analysis, respectively (Fig. 2D,E). Several genes associated with angiogenesis, including chemokine receptor CX3CR1 (also known as fractalkine), were also significantly downregulated. Significantly upregulated genes included Cdkn1a, which encodes the cyclin-dependent kinase inhibitor p21 (15). It is noteworthy that p21, a target of the tumor suppressor p53, was upregulated in these p53-mutant STSs with SU treatment. Upregulation of Cdkn1a/p21 was also confirmed by Quantitative reverse transcriptase PCR and Western blot analysis (Fig. 2D,E).

Treatment effects on tumor growth

We measured the tumor growth in the four treatment groups. The mean tumor size for all groups was 170 mm^3 at the onset of treatment. The tumors in the mice treated with carrier alone grew to a mean of 1378 ± 310 mm^3 after 12 days (Fig. 3A). The tumors of the mice treated with RT or SU averaged 810 ± 353 mm^3 ($p = .024$) and 600 ± 240 mm^3 ($p = .001$), respectively, after 12 days. The tumors in these two groups also appeared to be growing slowly when the mice were sacrificed. The tumors in the mice treated with both RT and SU were the smallest, averaging only 401 ± 90 mm^3 ($p < .0001$) at 12 days, 29% of the volume of the tumors treated with carrier alone. In addition, the tumors in this group were not growing when the mice were sacrificed.

Examination of cancer cell effects

The tumors were harvested after 12 days of treatment. Histologic tumor analysis after hematoxylin-eosin staining was performed by an experienced sarcoma pathologist (G.P.N.). The control tumors were all high-grade spindle cell and pleomorphic STSs resembling human high-grade undifferentiated STSs or malignant fibrous histiocytomas (Fig. 3B). These tumors were often infiltrative into the surrounding skeletal muscle. Tumors treated with RT had increased pleomorphism and contained large, hyperchromatic cells. SU-treated tumors had even more pleomorphism than the tumors treated with RT alone. These tumors also contained similar, large, hyperchromatic cells. The tumors treated with both RT and SU were also highly pleomorphic. Although untreated tumors often contained gross areas of central necrosis, only the tumors treated with both SU and RT contained focal areas of necrosis in apparently viable

areas of tumor (Fig. 3B, far right). Thus, according to routine histologic analysis, only the combination of SU and RT resulted in focal areas of necrotic cell death.

The use of RT and SU can affect tumor growth by decreasing cancer cell proliferation or increasing cell death. To determine whether these mechanisms might be involved in the tumor response, we examined the tumor sections for proliferation by proliferating cell nuclear antigen immunohistochemistry (Fig. 3B). Nearly all cancer cells in tumors treated with carrier alone showed proliferation by proliferating cell nuclear antigen staining, and tumor cells treated with RT alone or SU alone caused a 46–54% reduction in cancer cell proliferation (Fig. 3B,C). However, the greatest reduction in proliferation (77%) was observed in STSs treated with both SU and RT ($p < .0001$). To detect apoptosis, TUNEL immunofluorescence was performed. Control tumors showed little TUNEL staining (three tumor cell nuclei per high powered field). After treatment with RT alone or SU alone, on average, 11 and 14 TUNEL-positive nuclei per high powered field, respectively (Fig. 3B,D). STSs treated with both SU and RT showed dramatically increased apoptosis, with an average of 149 TUNEL-positive nuclei per high powered field ($p < .0001$).

Fluorescence-mediated tomographic imaging of tumor vasculature

Both SU and RT have known effects on endothelial cells and the formation and stability of tumor vasculature. AngioSPARK probes and an FMT imaging system were serially used to assess tumor vasculature and permeability *in vivo* before and after treatment in all mice treated in our study. Once the tumors became palpable, tumor-bearing mice were injected with AngioSPARK750 and imaged on the FMT system within 15 min. The mean fluorescence was equivalent in all groups before treatment (Fig. 4A,B). After treatment, the mice were injected with AngioSPARK680 and imaged. RT at 20 Gy when delivered in two 10-Gy fractions had no significant effect on mean fluorescence, and SU decreased mean fluorescence by 38% (Fig. 4A,B). The addition of RT to SU did not significantly decrease mean fluorescence further compared with SU alone.

Examination of effects on tumor vasculature and angiogenesis-related gene expression

The microvessel density of tumors was also analyzed by CD31 immunohistochemistry. RT (two doses of 10 Gy) resulted in mild reductions in microvessel density 6 days after RT, and SU markedly reduced microvessel density (Fig. 5A,B). The addition of RT (20 Gy) to SU did not significantly decrease the microvessel density further compared with SU treatment alone. To determine whether endothelial cells were undergoing apoptosis, we performed co-immunofluorescence with CD31 and TUNEL on tumor sections 7 days after RT (Fig. 5C). The largest numbers of apoptotic endothelial cells were present in tumors treated with both RT and SU compared with either alone.

Quantitative real-time PCR for a panel of pro-angiogenic factors was performed on tumors treated with SU and untreated tumors of similar size (Fig. 5D). VEGF expression, but not PDGF-α or PDGF-β expression, was significantly upregulated in tumors treated with SU (Fig. 5D). In addition, no significant differences were found on examination of basic fibroblast growth factor and angiopoietin 1 and 2 levels.

Discussion

The present study examined the effects of SU and/or RT in a genetically engineered mouse model of STS. Using a novel imaging system, we were able to assess treatment effects on tumor vasculature *in vivo* and found that SU decreased the mean fluorescence in tumors but RT had no effect. SU alone or RT alone delayed tumor growth, but maximal growth inhibition was

observed with combination therapy. The primary mechanism by which the combination of SU and RT inhibited tumor growth was by induction of tumor cell and endothelial cell apoptosis.

There could be some advantages in the use of genetically engineered mouse tumor models over explant models. Explant models, which generally involved the subcutaneous injection of murine cancer cell lines into syngeneic mouse strains or injection of human cancer cell lines into immunocompromised mouse strains, might not fully re-create the complex relationship between developing tumors and their host microenvironment. Therefore, the results of RT and biologic therapies in these models might not accurately predict the results in human cancer patients (16). For example, tumor endothelial cells isolated from xenografts of human tumors on a murine host demonstrate differential responses to VEGF compared with tumor endothelial cells isolated from oncogene-induced spontaneous tumors (17). Recent studies have demonstrated differential therapeutic effects of rapamycin on a xenograft tumor model vs. a spontaneous genetically engineered tumor model (18). These limitations might be especially relevant with drugs such as SU that target not only cancer cells but also the host-derived vasculature and tumor microenvironment.

Sunitinib and other targeted biologic agents act differently from traditional cytotoxic chemotherapeutic agents. Thus, alternative methods to radiologic evidence of tumor regression might be needed to assess drug activity during treatment. Using AngioSPARK intravascular probes and FMT imaging, we found that RT had little effect on mean fluorescence but that SU or SU plus RT significantly reduced mean fluorescence. These results corresponded to treatment effects on microvessel density, and thus FMT imaging might be an alternative to traditional dynamic contrast-enhanced magnetic resonance imaging (19) or perfusion computed tomography (20) in assessing the effects of anti-angiogenic agents on tumors. Other new technologies such as contrast ultrasonography with microbubbles show great promise in evaluating the effects of anti-angiogenic agents *in vivo* (21).

We tried to separately examine the effects of SU on cancer cells and the effects on tumor vasculature, although these effects are interconnected. In terms of cancer cell effects, SU increased the expression of the cyclin-dependent kinase inhibitor p21, which correlated with decreased cancer cell proliferation. The decrease in cancer cell proliferation with combination therapy appeared to be additive and not synergistic. The combination of SU and RT inhibited tumor growth by way of the induction of cancer cell apoptosis, and this effect was clearly synergistic. The levels of cancer cell apoptosis as measured by TUNEL staining were 10-fold greater with combination therapy than with either therapy alone. Cancer cells isolated from tumors were analyzed using an *in vitro* clonogenic survival assay in the presence or absence of 1 μM SU. Although SU inhibited VEGFR-2 phosphorylation at this concentration (Fig. E2a), SU had no effect on clonogenic survival *in vitro* (Fig. E2b), suggesting that SU augments RT primarily through changes in the tumor microenvironment rather than by direct effects on the cancer cells.

The mechanisms by which SU could limit tumor angiogenesis include inhibition of endothelial cell proliferation, induction of endothelial cell apoptosis, and inhibition of pericyte coverage of immature vessels. Seven days after 20 Gy (10 Gy × 2), RT alone had had only a minor effect on microvessel density and endothelial cell-specific apoptosis, but SU had profoundly reduced the microvessel density and caused some degree of endothelial cell apoptosis. In another study, SU induced apoptosis in human umbilical vein endothelial cells *in vitro*, but SU treatment of implanted gliomas resulted in no endothelial cell apoptosis *in vivo* (22).

Our study had several limitations. First, >50 different histologic subtypes of human STSs exist, and any one mouse model will not account for this diversity. However, the tumors formed in the genetically engineered mouse model used in the present study histologically resemble one

of the most common human STSs: high-grade undifferentiated sarcoma or malignant fibrous histiocytoma (7). Second, the imaging modality used in this study, FMT with pegylated nanoparticles coupled to a near-infrared fluorochrome, is a new modality, and only two points were measured (before treatment and at the end of treatment). Exactly how much fluorescence resulted from an intravascular probe vs. a probe that had leaked out of tumor vessels is unknown. Nanoparticles have been demonstrated to have enhanced permeability and retention within tumors (20), and RT has been shown to increase the enhanced permeability and retention of tumors (21). To address this issue, additional studies of FMT using these imaging probes in this mouse model are needed. Third, although the present study analyzed the effects of sunitinib and/or RT using a wide variety of modalities, clearly additional analyses can be performed. For example, our analysis of global gene expression changes in tumors and our analysis of specific changes in angiogenesis-related genes could pave the way for the discovery of predictive biomarkers of the treatment response.

Conclusion

The results of the present study have added to the limited preclinical data on the efficacy of combining SU and RT in the treatment of solid tumors. In contrast, numerous preclinical studies (22) and at least 1 human study (23) have demonstrated that specific inhibition of the VEGF pathway enhances the efficacy of RT. SU targets the VEGF pathway, along with other pathways involved in tumor growth and angiogenesis; thus, the combination of SU and RT might be equal to, or better than,. the combination of bevacizumab and RT. Owing to the encouraging results from the present study and other preclinical studies, the combination of SU and RT should be investigated in future clinical trials.

Supplementary Material

Refer to Web version on PubMed Central for supplementary material.

Acknowledgments

Approved and funded by the National Comprehensive Cancer Network from general research support provided by Pfizer, Inc., and supported by the Howard Hughes Medical Institute (T. Jacks) and partially by several grants from the National Cancer Institute: Grants K12 CA 87723-03 (S. S. Yoon), P50 CA86355 (R. Weissleder), U54 CA119349 (R. Weissler, T. Jacks), U24 CA92782 (R. Weissleder), KO8 CA 114176 (D. G. Kirsch), RSNA Holman Pathway Resident Seed Grant (D. G. Kirsch), and P30-CA14051 (T. Jacks). T. Jacks is the David H. Koch Professor of Biology and a Daniel K. Ludwig Scholar.

References

1. Nieder C, Wiedenmann N, Andratschke NH, Astner ST, Molls M. Radiation therapy plus angiogenesis inhibition with bevacizumab: rationale and initial experience. Rev Recent Clin Trials 2007;2:163–168. [PubMed: 18474001]
2. Mendel DB, Laird AD, Xin X, et al. In vivo antitumor activity of SU11248, a novel tyrosine kinase inhibitor targeting vascular endothelial growth factor and platelet-derived growth factor receptors: Determination of a pharmacokinetic/pharmacodynamic relationship. Clin Cancer Res 2003;9:327–337. [PubMed: 12538485]
3. Faivre S, Demetri G, Sargent W, et al. Molecular basis for sunitinib efficacy and future clinical development. Nat Rev Drug Discov 2007;6:734–745. [PubMed: 17690708]
4. Yoon SS, Segal NH, Park PJ, et al. Angiogenic profile of soft tissue sarcomas based on analysis of circulating factors and microarray gene expression. J Surg Res 2006;135:282–290. [PubMed: 16603191]
5. Cuneo KC, Geng L, Fu A, et al. SU11248 (sunitinib) sensitizes pancreatic cancer to the cytotoxic effects of ionizing radiation. Int J Radiat Oncol Biol Phys 2008;71:873–879. [PubMed: 18514780]

6. Schueneman AJ, Himmelfarb E, Geng L, et al. SU11248 maintenance therapy prevents tumor regrowth after fractionated irradiation of murine tumor models. Cancer Res 2003;63:4009–4016. [PubMed: 12873999]
7. Kirsch DG, Dinulescu DM, Miller JB, et al. A spatially and temporally restricted mouse model of soft tissue sarcoma. Nat Med 2007;13:992–997. [PubMed: 17676052]
8. Montet X, Figueiredo JL, Alencar H, et al. Tomographic fluorescence imaging of tumor vascular volume in mice. Radiology 2007;242:751–758. [PubMed: 17325064]
9. Detwiller KY, Fernando NT, Segal NH, et al. Analysis of hypoxia-related gene expression in sarcomas and effect of hypoxia on RNA interference of vascular endothelial cell growth factor A. Cancer Res 2005;65:5881–5889. [PubMed: 15994966]
10. Ryeom S, Baek KH, Rioth MJ, et al. Targeted deletion of the calcineurin inhibitor DSCR1 suppresses tumor growth. Cancer Cell 2008;13:420–431. [PubMed: 18455125]
11. Kruskal WH, Wallis A. Use of ranks in one-criterion variance analysis. J Am Stat Assoc 1952;47:583–621.
12. Rae F, Woods K, Sasmono T, et al. Characterisation and trophic functions of murine embryonic macrophages based upon the use of aCsf1r-EGFP transgene reporter. Dev Biol 2007;308:232–246. [PubMed: 17597598]
13. Wagner M, Klussmann JP, Fangmann R, et al. Cyclin-dependent kinase-inhibitor 1 (CDKN1A) in the squamous epithelium of the oropharynx: possible implications of molecular biology and compartmentation. Anticancer Res 2001;21:333–345. [PubMed: 11299759]
14. Gutmann DH, Hunter-Schaedle K, Shannon KM. Harnessing preclinical mouse models to inform human clinical cancer trials. J Clin Invest 2006;116:847–852. [PubMed: 16585951]
15. Phung TL, Ziv K, Dabydeen D, et al. Pathological angiogenesis is induced by sustained Akt signaling and inhibited by rapamycin. Cancer Cell 2006;10:159–170. [PubMed: 16904613]
16. Johannessen CM, Johnson BW, Williams SM, et al. TORC1 is essential for NF1-associated malignancies. Curr Biol 2008;18:56–62. [PubMed: 18164202]
17. O'Connor JP, Jackson A, Parker GJ, et al. DCE-MRI biomarkers in the clinical evaluation of antiangiogenic and vascular disrupting agents. Br J Cancer 2007;96:189–195. [PubMed: 17211479]
18. Sahani DV, Kalva SP, Hamberg LM, et al. Assessing tumor perfusion and treatment response in rectal cancer with multisection CT: Initial observations. Radiology 2005;234:785–792. [PubMed: 15734934]
19. Ellegala DB, Leong-Poi H, Carpenter JE, et al. Imaging tumor angiogenesis with contrast ultrasound and microbubbles targeted to alpha(v)beta3. Circulation 2003;108:336–341. [PubMed: 12835208]
20. Cho K, Wang X, Nie S, et al. Therapeutic nanoparticles for drug delivery in cancer. Clin Cancer Res 2008;14:1310–1316. [PubMed: 18316549]
21. Li C, Ke S, Wu QP, et al. Tumor irradiation enhances the tumor-specific distribution of poly(l-glutamic acid)-conjugated paclitaxel and its antitumor efficacy. Clin Cancer Res 2000;6:2829–2834. [PubMed: 10914731]
22. Wachsberger P, Burd R, Dicker AP. Tumor response to ionizing radiation combined with antiangiogenesis or vascular targeting agents: exploring mechanisms of interaction. Clin Cancer Res 2003;9:1957–1971. [PubMed: 12796357]
23. Willett CG, Boucher Y, di Tomaso E, et al. Direct evidence that the VEGF-specific antibody bevacizumab has antivascular effects in human rectal cancer. Nat Med 2004;10:145–147. [PubMed: 14745444]

A

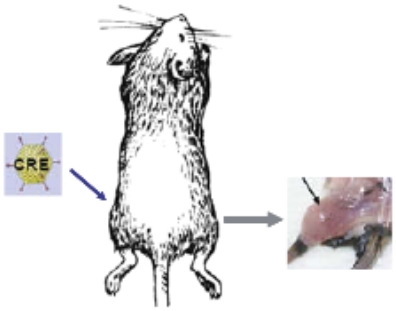

B

Genotype	Sarcoma incidence	Days to tumor Range (median)
LSL-Kras^{G12D};p53$^{LSL.R270H/Fl}$	2/2 (100%)	72-100 (86)
LSL-Kras^{G12D};p53$^{LSL.R172H/Fl}$	6/7 (85%)	72-121 (93.5)
LSL-Kras^{G12D};p53$^{Fl/Fl}$	14/15 (93%)	69-121 (83)

C

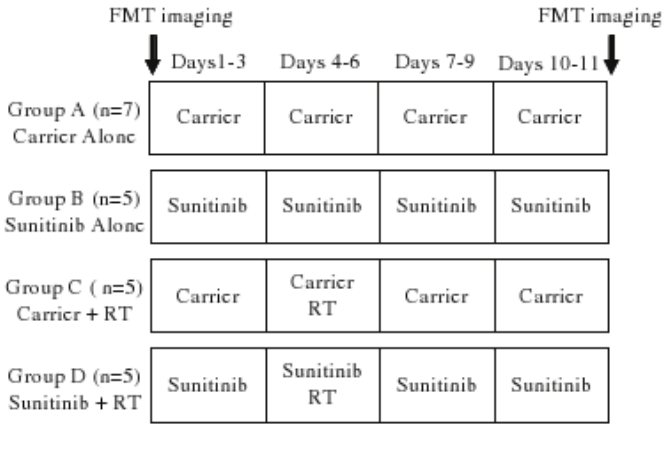

Fig. 1.

Generation and treatment of primary sarcomas induced in genetically engineered mice. (A) Schematic diagram demonstrating generation of extremity soft-tissue sarcomas in mice with conditional mutations in K-ras and p53. Black arrow points to extremity sarcoma. (B) Table showing genotype of mice, sarcoma incidence, and interval in days to tumors developing. (C) Schematic diagram demonstrating treatment of randomized mice. RT = radiotherapy; FMT = fluorescence-mediated tomography.

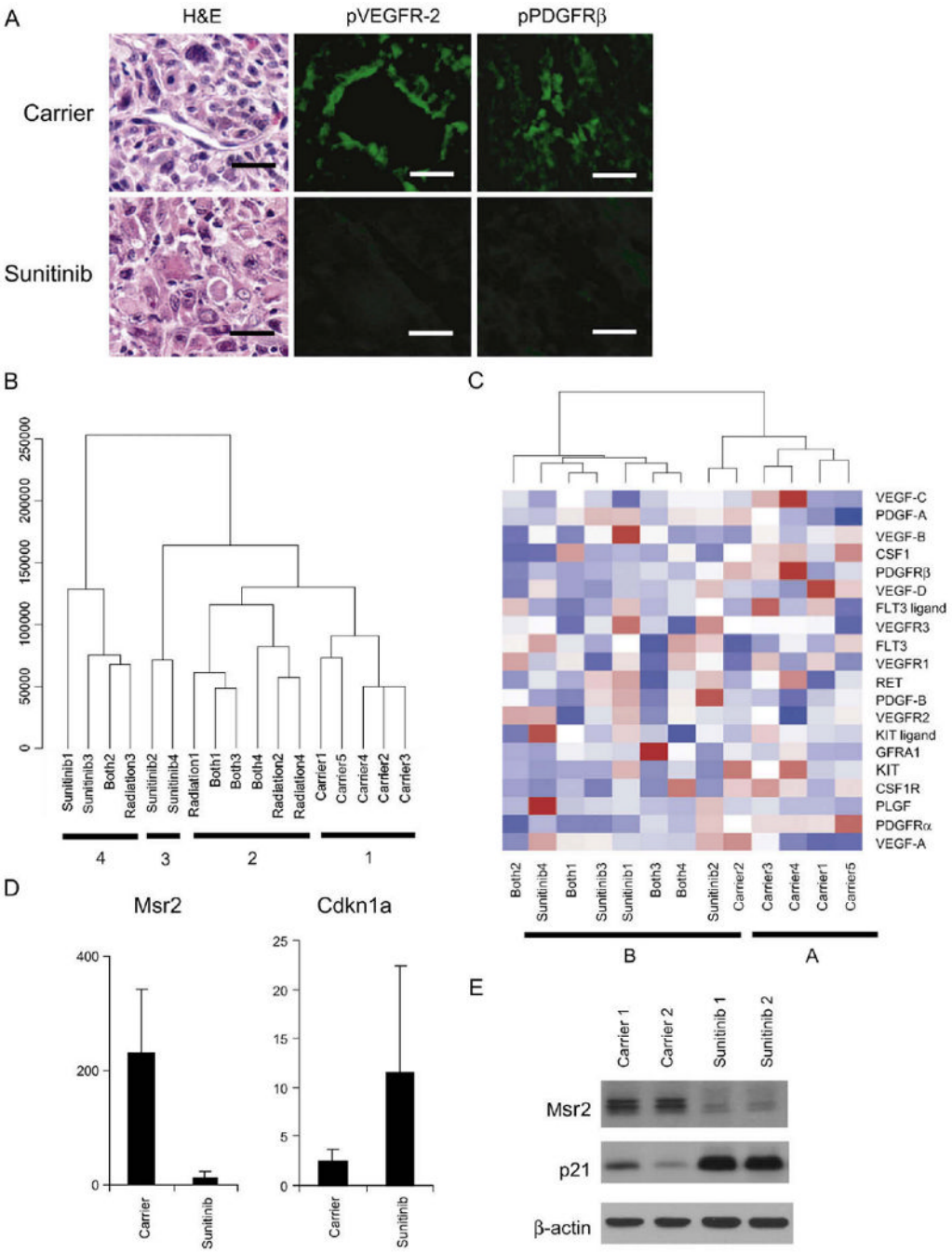

Fig. 2.

Effects of sunitinib on target receptors and gene expression. (A) Hematoxylin-eosin images and immunofluorescence images for phosphorylated vascular endothelial growth factor receptor (pVEGFR-2, green) or phosphorylated platelet-derived growth factor receptor-*β* (PDGFR*β*, green). Scale bar, 20 *μ*m. (B) Dendrogram following hierarchical clustering of tumors using 500 most variable genes. (C) Dendrogram and heat map following hierarchical clustering using only 20 sunitinib-related genes. Blue represents high expression, white moderate, and red low. (D) Quantitative reverse transcriptase polymerase chain reaction (RT-PCR) for macrophage scavenger receptor (Msr2) and Cdkn1a (p21) in tumors treated with

carrier vs. sunitinib. Bars represent standard deviation. (E) Western blot analysis of MSR2 and p21 levels. β-actin levels served as loading control.

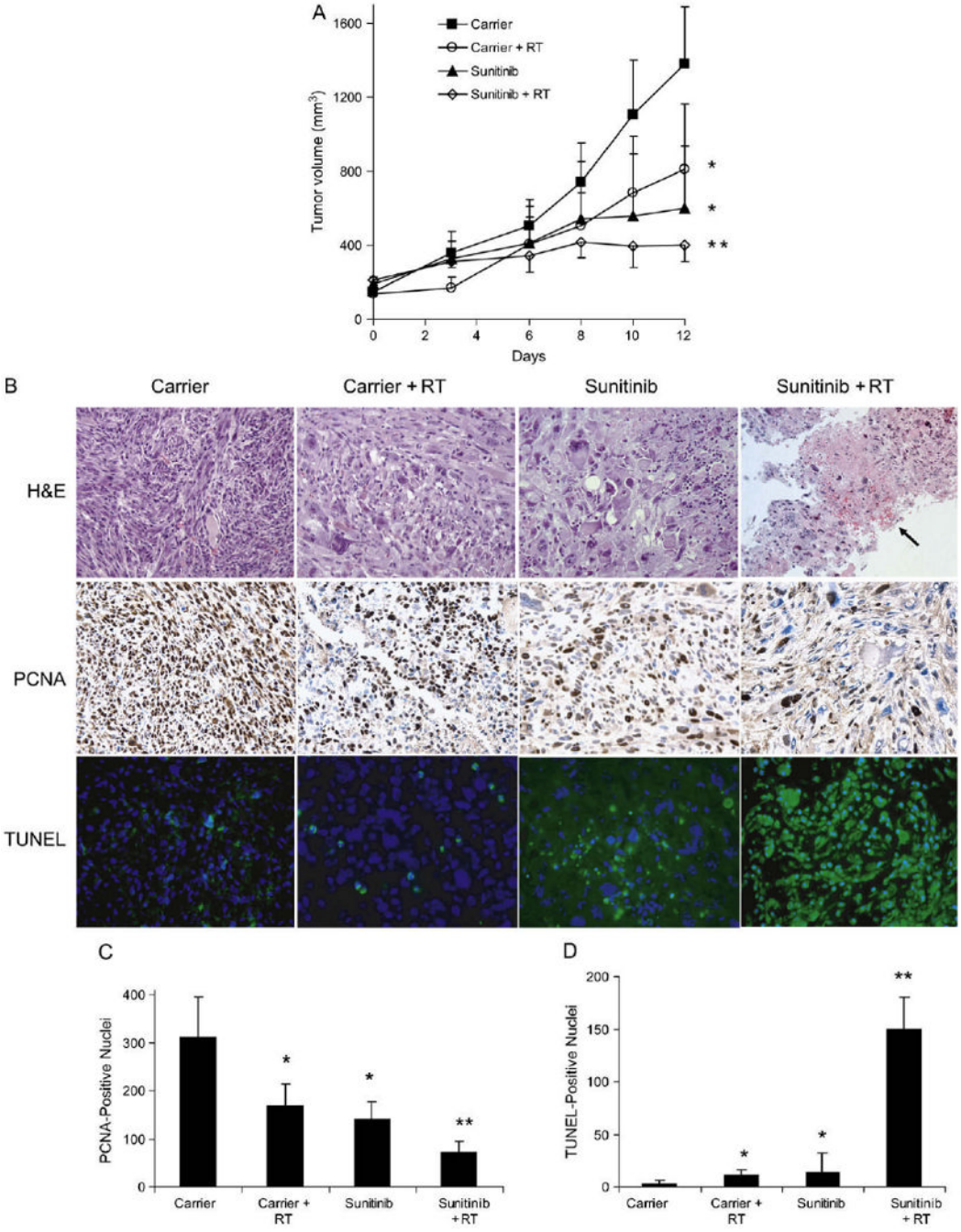

Fig. 3.

Treatment effects on tumor size and cancer cells. (A) Tumor growth curve of four treatment groups. RT = radiotherapy. (B) Representative hematoxylin-eosin (H&E), proliferating cell nuclear antigen (PCNA), and terminal deoxynucleotidyl transferase-mediated dUTP-biotin nick end labeling (TUNEL) images of tumors treated with carrier, RT, sunitinib, or both RT and sunitinib. Arrow points to area of focal necrosis. Scale bar, 100 μm. (C) PCNA-positive nuclei per 5 high-powered fields. (D) TUNEL-positive nuclei per 5 high-powered fields. Bars represent standard deviation. *p <.05 compared with carrier group. **p <.05 compared with 3 other groups.

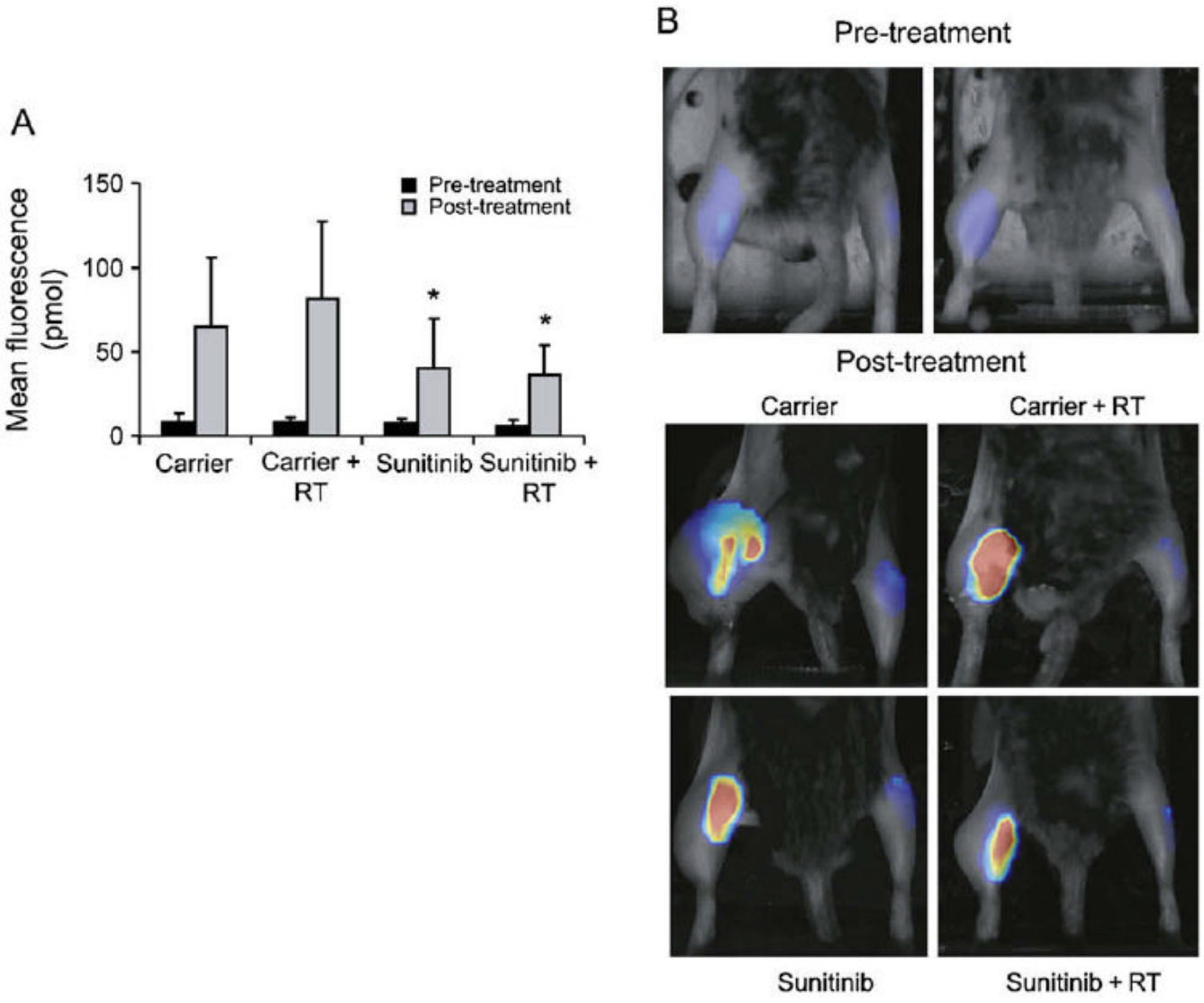

Fig. 4.

Fluorescence-mediated tomography. (A) Mean fluorescence after intravenous injection with intravascular probes (AngioSPARK680 or AngioSPARK750) and (B) representative images before and after treatment. RT = radiotherapy. Bars represent standard deviation. *p <.05 compared with carrier group.

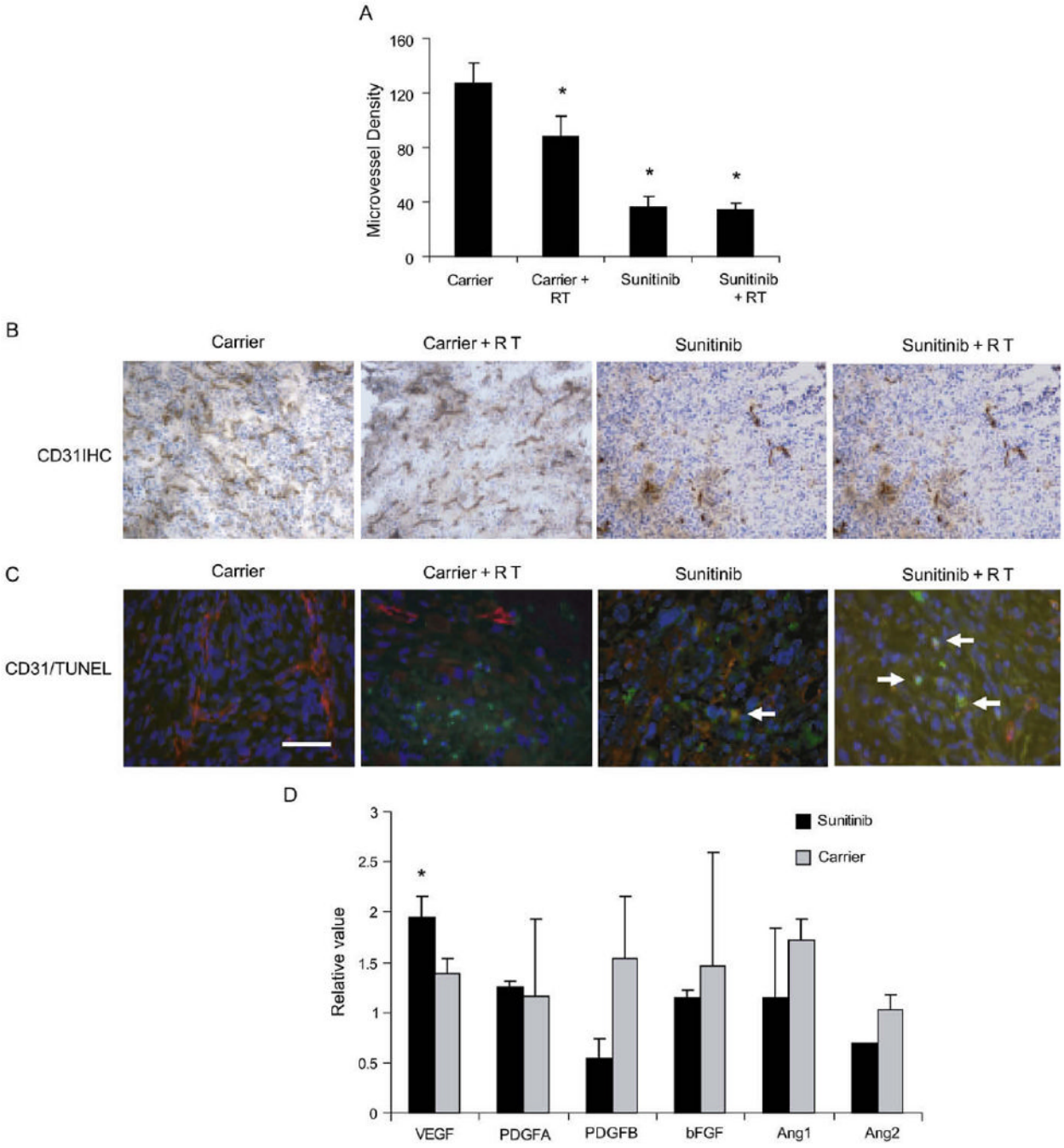

Fig. 5.

Treatment effects on tumor vasculature. (A) Microvessel density after immunohistochemical staining for CD31. RT = radiotherapy. (B) Representative images of CD31 immunohistochemistry (IHC). Scale bar, 100 μm. (C) Terminal deoxynucleotidyl transferase-mediated dUTP-biotin nick end labeling (TUNEL) (green)/CD31 (red)/Hoechst (blue) immunofluorescence. White arrows indicate cells with co-localization of TUNEL and CD31. Scale bar, 20 μm. (D) Quantitative real-time polymerase chain reaction of carrier and sunitinib-treated tumors for vascular endothelial growth factor (VEGF), platelet-derived growth factors A and B (PDGF-A, PDGF-B), basic fibroblast growth factor (bFGF), and angiopoietins 1 and 2. *p <.05 compared with carrier group.